ANTIOXIDANTS & REDOX SIGNALING
Volume 9, Number 10, 2007

DOI: 10.1089/ars.2007.1717

Forum Review

Methods for Noninvasive Imaging of Tissue Hypoxia

DEEPTI S. VIKRAM, JAY L. ZWEIER, and PERIANNAN KUPPUSAMY

ABSTRACT

The purpose of this review is to provide an overview of the methods available for imaging tissue oxygenation. The following imaging methods are reviewed: phosphorescence, near-infrared (NIR), positron emission tomography (PET), magnetic resonance imaging (^{19}F MRI and BOLD MRI), and electron paramagnetic resonance (EPR). The methods are based on different principles and differ in their ability to accurately quantify tissue oxygenation, either the absolute value of a particular measure of oxygenation (partial pressure of oxygen, concentration), or a parameter related to it (oxygen saturation). Methods that can provide images of relative changes in oxygenation or visualization of hypoxia in a specific tissue of interest are also considered valuable tools for biomedical research and clinical applications. *Antioxid. Redox Signal.* 9, 1745–1756.

INTRODUCTION

Oxygen is an essential part of metabolism and the electron transport chain in the mitochondria of living cells. Any imbalance in the oxygen levels, which may occur due to altered supply or utilization of oxygen, may affect the metabolic homeostasis and lead to pathophysiological diseases (1, 17, 52). Thus, a precise knowledge of the levels of oxygen in the tissue of interest will be of paramount importance in our ability to understand the mechanism of pathogenesis and to develop strategies to correct the imbalance. This would require methods capable of quantifying the levels of tissue oxygenation with good spatial and temporal resolution. The information gained will enable better understanding of various metabolic and disease states (*e.g.*, cancer and peripheral vascular disease) and help in making effective clinical decisions regarding treatment and therapy.

The chemical and physical properties of oxygen enable a wide variety of methods for measuring and mapping oxygen content *in vivo*. The choice of any method should be based on its applicability and the nature of information sought. There are many reviews on the methods of oxygen measurement techniques and their applications to specific organs and diseases (19, 79). However, this review article will focus on some of the methods that are used for imaging (mapping) oxygen content. The intent is to provide a comparative description and evaluation of the techniques (with emphasis on electron paramagnetic resonance imaging) as well as highlight some of the applications where they will be found to be most useful.

Even though the discovery of oxygen was made in the 18th century, measurements of oxygen concentration in living systems (*in vivo*) are only a recent phenomenon. Early attempts were made in the 1960s (14, 43) but it was in the late 1980s that the computerized polarographic needle electrode system was used to assess the oxygenation in tumors clinically (80). The use of this technique helped to establish the role of hypoxia in ineffective radio- or chemotherapy (11, 12, 32, 33, 61). Now there are several methods that are based on other principles, including fluorescence quenching, phosphorescence, optical detection, immunohistochemical, and magnetic resonance techniques. Though all the methods report useful information about oxygenation in tissue, not all of them are capable of mapping (imaging) the oxygen content in tissue. The advantages of imaging oxygen over single-site measurements are obvious. Since oxygen is not involved in just one physiological process, characterizing the heterogeneity of oxygen distribution over the region of interest (*e.g.*, tumor, heart) helps in the investigation of the underlying pathophysiology, as well as making clinical treatment more effective.

Center for Biomedical EPR Spectroscopy and Imaging, Comprehensive Cancer Center, Davis Heart and Lung Research Institute, Department of Internal Medicine, The Ohio State University, Columbus, Ohio.

In general, the methods for imaging of oxygen can be broadly categorized into three groups: (a) optical methods: near-infrared spectroscopy (NIRS) and phosphorescence; (b) nuclear medicine methods: positron emission tomography (PET); and (c) magnetic resonance-based methods: blood oxygen level-dependent magnetic resonance imaging (BOLD MRI); ^{19}F MRI; electron paramagnetic resonance imaging (EPRI), and proton–electron double resonance imaging (PEDRI). Some of the desirable criteria for the successful imaging of oxygenation in living systems are: (a) noninvasiveness; (b) capability to make repeated measurements; (c) accessibility to the region of interest; (d) image resolution; (e) depth of measurement; (f) accu-

TABLE 1. COMPARISON OF THE METHODS OF OXYGEN IMAGING

	EPRI	*BOLD MRI*	*19 F MRI*	*PET*	*Phosphorescence imaging*	*NIRS*
Category	Magnetic resonance	Magnetic resonance	Magnetic resonance	Nuclear	Optical	Optical
Probe	Soluble, particulate	None	Perfluro-carbons (PFCs)	^{18}F-MISO, ^{18}F-EF5	Phosphors (external)	None
Probe size	Soluble: single molecule Particulate: 100–500 μm	NA	50 μL injection	Single molecule	<3 mg/kg	NA
Oxygen consumption	No	No	No	No	No	No
Interference from other sources	No	Signal interpretation	No, high specificity	Possible binding to aerobic cells	No, high specificity	No
Mode	Spatial temporal	Spatial temporal	Spatial temporal	Spatial temporal	Spatial and temporal	Spatial temporal
Data acquisition time	Minutes, hours	Method dependent	About 150 readings in ~7 min	Minutes, hours	?	?
Range	0–100 mm Hg	Relative pO_2	0–760 mm Hg	0–10 mm Hg	0–160 mm Hg (at least)	?
Sensitivity	<1 mm Hg		1–3 mm Hg	<10 mm Hg to detect tracer (^{18}F-MISO), high for ^{18}F-EF5		
Resolution	0.5 mm	Comparable to conventional MRI		Linear 2 mm (FMIS O), 6–8 mm for human studies	50 micron with blue, less with other wavelengths	Spatial: 2 mm–cm Temporal: 50 ms-min
Lifetime	Soluble probes: several min Particulate probes: months	NA	Half life 600 min ^{18}F-EF5	^{18}F-MISO: 1.83 hrs ~12 h	μsec (Green 2W and Pd-porphyrin)	NA
Invasive/non-invasive	Minimally invasive	Noninvasive	Minimally noninvasive	Minimally invasive	Minimally invasive	Noninvasive
Calibration needed	Yes	Yes	Yes, in vitro calibration	Yes	Yes	Yes
Specificity	High	Issues	High specificity	Issues with specificity	High	Hb, Mb, cytochrome oxidase
Thickness of tissue accessib le	cm	No limit	No limit	No limit	Cm of tissue	cm
Repetitive measurements	Yes	Yes	Yes	Yes	Yes	Yes

racy and robustness of measurements; (g) usefulness of the parameter reported and its clinical utility; (h) background noise in image; (i) image acquisition time; (j) ease of use; and (k) commercial or potential availability of the instrumentation. It is important that the method should enable repeated measurements from the region of interest to follow the changes in oxygenation over a period of time, preferably for up to several weeks. The technique should also provide good spatial and temporal resolution. The depth of measurement (penetration) and accessibility to the region of interest are some of the important factors for the scope of applicability of the technique. All the imaging techniques do not report the same parameter which should be taken into account when deciding the usefulness of the technique. These points will be further discussed with respect to each technique presented in the following sections.

METHODS FOR IMAGING OF TISSUE OXGENATION

The purpose of this review is to provide an overview of the various methods available for imaging tissue oxygenation. The following methods are reviewed: phosphorescence imaging, near-infrared spectroscopy, positron emission tomography imaging, magnetic resonance imaging, and electron paramagnetic resonance imaging. A comparative evaluation of their principle, applicability, advantages, and limitations is given in Table 1. It should be noted that although tissue oxygenation is generally referred to as oxygen tension or partial pressure of oxygen (pO_2, in units of mm Hg or Torr), other terminologies such as oxygen concentration (μM) and percent oxygen (% O_2) are also used. These measures correspond to free (unbound) molecular oxygen. Since free molecular oxygen will be in equilibrium with bound oxygen, for example, in oxyhemoglobin or oxymyoglobin, oxygen saturation is also used as a measure of tissue oxygenation. Most often, the difference in the terminology of oxygenation is also due to the differences in the method of oxygen measurement used. Thus, it is pivotal to establish the validation of each method in the context of other methods to ensure that the measured data is meaningfully interpreted.

Phosphorescence imaging

Oxygen detection by phosphorescence-quenching has now been in use for >15 years (70, 84). Measurement of oxygen using the phosphorescence quenching technique involves the injection of a phosphor material into the vasculature. A bifurcated light guide is used to focus the excited light from the source to the surface of the tissue where it is detected by a phosphorometer. This technique is gaining importance for *in vivo* applications (26, 85) as further technical and probe improvements are continuously being made (71, 82).

The phosphorometer (detector) utilizes photomultipliers or avalanche photodiodes (75) to measure the phosphorescence signal to get information about the distribution of the lifetimes

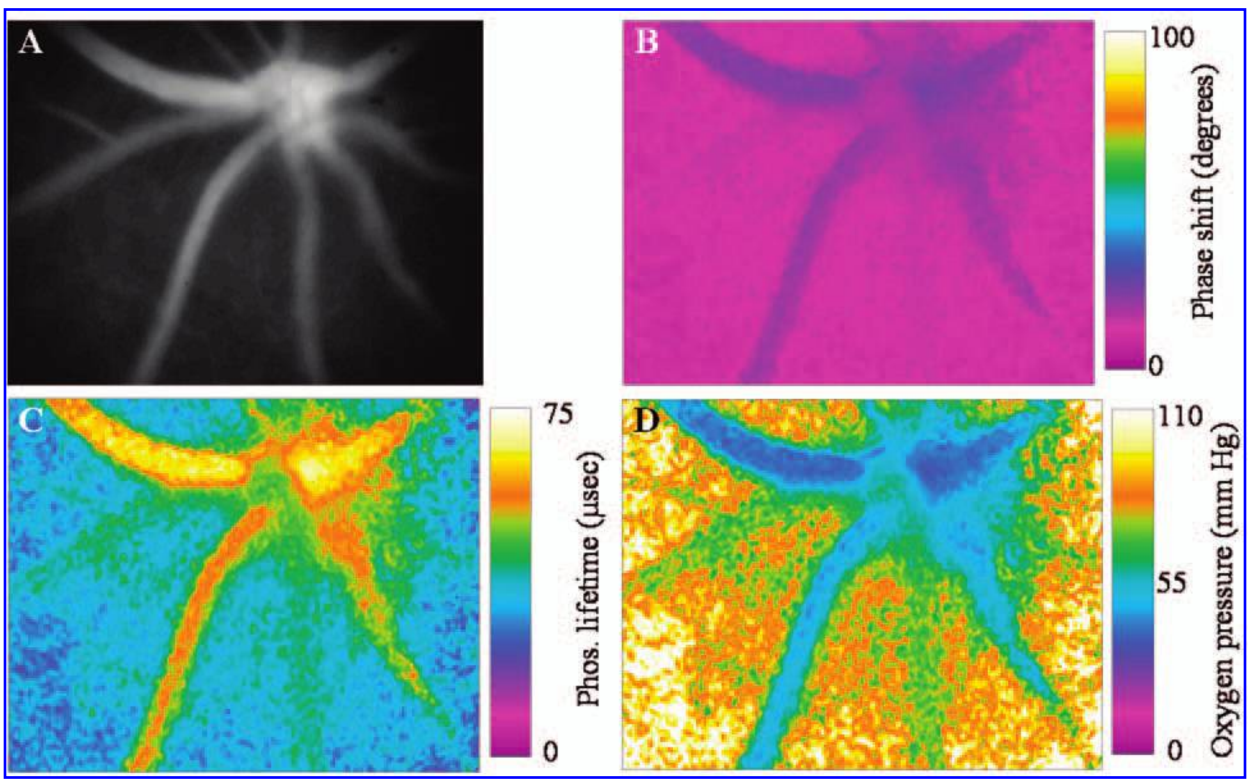

FIG. 1. Oxygen map of the retina using phosphorescence imaging. The images show the effect of anesthesia on retinal (mouse) oxygen pressures with time. Phase delay images (**A** and **B**), phosphorescence-lifetime image (**C**), and oxygen pressure image (**D**) are shown. Reproduced with permission from Wilson *et al*. (92). (For interpretation of the references to color in this figure legend, the reader is referred to the web version of this article at www.liebertonline.com/ars)

and amplitudes of the phosphor probe. Data analysis involving calibration, and deconvolution subsequently gives histogram representations of pO_2 over the sampled region. When the measurements are done in a grid pattern, it is possible to construct contour maps that contain the volume fraction of tissue sampled for any selected range of pO_2 values (84). The phosphorimeters can work in time or frequency domains (83), but frequency-lock techniques are reported to be stable, with insensitivity to ambient light (84).

The method requires the infusion of water-soluble phosphor probes into the vasculature. The phosphors (*e.g.*, Oxyphor G2, Green 2W, and Pcl-porphyrin), absorb in the near-infrared region of 620–1,000 nm (90). There is low absorbance by natural pigments in this spectral window, thereby giving high specificity to the method. The most widely used probe for *in vivo* applications is Pcl-meso-tetra(4-carboxyphenyl)porphyrin which has a lifetime of 650 μsec (90). Phosphorescence imaging has several advantages: (a) near-infrared light can penetrate a substantial thickness of tissue, from a few mm to cm (84, 90); (b) the technique can produce a histogram for each measurement; (c) "real time" measurements, with the added advantage of repeated measurements are possible; (d) the temporal resolution is a few seconds or less (84); (e) construction of contour maps of the volume fraction of hypoxic tissue in each region of tissue is possible (84); (f) the method gives an accurate representation of size and visualization of changes in oxygenation (spatially and temporally); (g) rapid response time (msec), wide dynamic range, accuracy in low pO_2, and high specificity are the other advantages of this technique.

One of the limitations of the phosphorescence method is that the technique requires injection of an external probe (phosphor) in the vasculature and the reported parameter is vascular pO_2, not tissue pO_2. Therefore, comparisons with other methods, especially with nonvasculature imaging methods are required for correct interpretation.

Phosphorescence imaging has been widely used for mapping the oxygenation concentration in tumors (26, 87, 88), retinas (71, 91), mouse vasculature (49), hearts (69), and brains (26, 89). An example of an oxygen map generated using this technique is shown in Fig. 1 for a mouse retina (92).

Near-infrared spectroscopy

Near-Infrared Spectroscopy (NIRS) was first demonstrated in 1977 by Jobsis for assessing the adequacy of the oxygen supply and consumption in living tissues (37). Now, NIRS is widely used as a research tool to investigate dynamic changes in tissue oxygenation by measuring hemoglobin (Hb) saturation (10). Like phosphorescence techniques, NIRS uses visible light (700–1,000 nm) in the near-infrared region which passes readily through biological tissues, bone, and muscle (10). The energy in this range is absorbed by Hb, myoglobin (Mb), and cytochrome c oxidase (10). In muscle tissue, the absorption is mostly by Hb, while ~10% is by Mb, and 2–5% is by cytochrome c oxidase (9). Thus, the NIRS signal is obtained primarily from the absorption of light by hemoglobin in the vasculature (small arterioles, capillaries, and venules). The absorption is minimal in small vessels while large vessels completely absorb the light, so the vascular specificity comes from the differential light absorption between large and small blood vessels (9). Since the absorption spectra of oxyhemoglobin and deoxyhemoglobin are different, the concentrations of these species can be determined by recording the spectral changes and then fitting the relative absorbances to the spectra of the chromophores (22).

The NIRS technique is noninvasive, with excellent temporal resolution, low-cost, and portability (36). For clinical studies, this method can be used under normal conditions without a major restriction of motion. The biggest advantage is the ability to perform real-time measurements and their repeatability, so that treatment as well as progression of the pathologic condition (such as stroke) can be investigated (36).

One drawback of the NIRS method is that it does not measure tissue pO_2. It provides information on vascular oxygenation (oxygen saturation) which indicates the balance between oxygen delivery and oxygen consumption (9). The light scatter

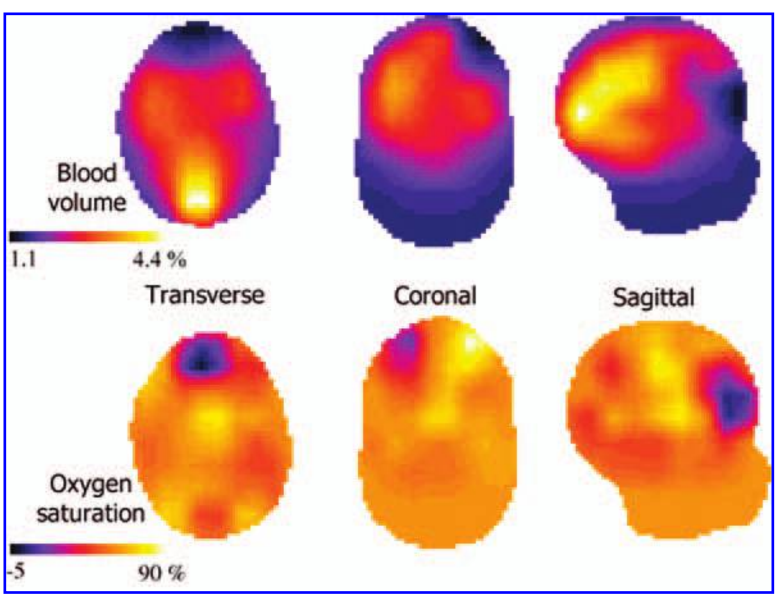

FIG. 2. NIRS oxygenation images of the infant brain. Transverse, coronal, and sagittal slices from 3D infant brain. The images show the estimated blood volume and fractional oxygen saturation. Reproduced with permission from Hebden et al. (30). (For interpretation of the references to color in this figure legend, the reader is referred to the web version of this article at www.liebertonline.com/ars)

and path-length may be constant within a subject, but there might be inter-subject variability (9). Also, modeling is required to estimate the path-length and consequently, the absorption coefficient of the tissue. This is difficult in clinical applications where the exact tissue boundaries need to be established. In addition, there are issues with the estimation of path length and modeling for heterogeneous tissues (22). The spatial resolution of NIRS is limited due to diffuse light measurements, although reconstruction methods have undergone improvement (22).

NIRS is used for clinical studies of peripheral vascular disease and studies involving muscle oxygenation, especially in the area of exercise physiology. In the clinical setting, NIRS is used for cerebral oxygenation and blood flow measurements (39, 72). NIRS is a valuable tool for monitoring ischemic and hemorrhagic stroke. Some of the reviews on this technique are by Intes *et al*. (36), Boushel *et al*. (9, 10), and Dunn *et al*. (22). Figure 2 shows images of oxygenation obtained using NIRS in the infant brain.

NIRS was compared with blood oxygen level-dependent (BOLD) imaging, which is described in this article later. A good correlation between the relaxation rate (R_2*) and deoxyhemoglobin content in the brain tissue was observed (38, 64). Further comparisons showed good spatial correlation between the two methods during task-oriented studies (15, 22). Comparison of NIRS with ^{19}F MRI (described in the following section) has also been reported (93).

PET imaging

Positron emission tomography (PET) uses short-lived positron emitting radionuclides for *in vivo* imaging of a variety of biomarkers (molecules). Researchers at Washington University (St. Louis, MO) and Searle Radiographers (Des Plains, IL) developed instrumentation that could be used for *in vivo* imaging of the positron-emitting radionuclides (5, 16). The PET/CT (computed X-ray tomography) combined modality is gaining importance as it has the added advantage of obtaining anatomical information along with PET data. Imaging of oxygen using PET involves the introduction of a class of probes called hypoxia markers. The probes are ^{18}F-containing imidazoles (*e.g.*, ^{18}F fluoromisonidazole, FMISO) which bind to intracellular macromolecules in hypoxic cells. Several radiotracers or biomarkers have been used for tumor hypoxia imaging, including FMISO and ^{18}F-containing a pentafluorintated derivative of etanidazole (EF5). A list of these radio-labeled compounds that have been used in animal models is given by Krause *et al*. (44).

The most widely used and investigated tracer is FMISO (41, 42, 66). The 2-nitroimidazoles are a class of compounds that have maximum binding to severely hypoxic cells (<0.38 mm Hg of oxygen, for example) and increased inhibition to increasing oxygenation dictated by Michaelis–Menton kinetics. They can also be radiolabeled and used for PET imaging of hypoxia (40). It has been reported that the covalent binding of FMISO to cellular macromolecules is 28 times higher in hypoxic environments as compared to normoxic conditions (67). No accumulation occurs in regions with a median pO_2 of >10 mm Hg (67). Studies have shown that the binding of FMISO occurs between oxygen levels of 2–10 mm Hg (62, 63). The probe is injected intravenously resulting in a low patient dose of 0.0126 mGy/MBq (28). Hypoxia imaging is usually performed 90–120 min after the i.v. injection, as FMISO distribution immediately after injection provides information about tumor perfusion while the effects due to hypoxia are observed later. Analysis of the collected data gives a tissue/blood ratio or tumor/muscle ratio, which is used for interpretation of the oxygenation status in tumors (42, 95). The initial clearance time of FMISO is from 5 to 10 h (42). So, the marker will be present in tumors long enough for extensive bioreduction and linkage of a higher radioactive signal to viable hypoxic cells (16). High stability, high safety, and availability has contributed to its wide usage (31, 41, 50, 65).

EF5 is another example of a hypoxia marker and has a uniform biodistribution and stable structure *in vivo* (40). Detailed

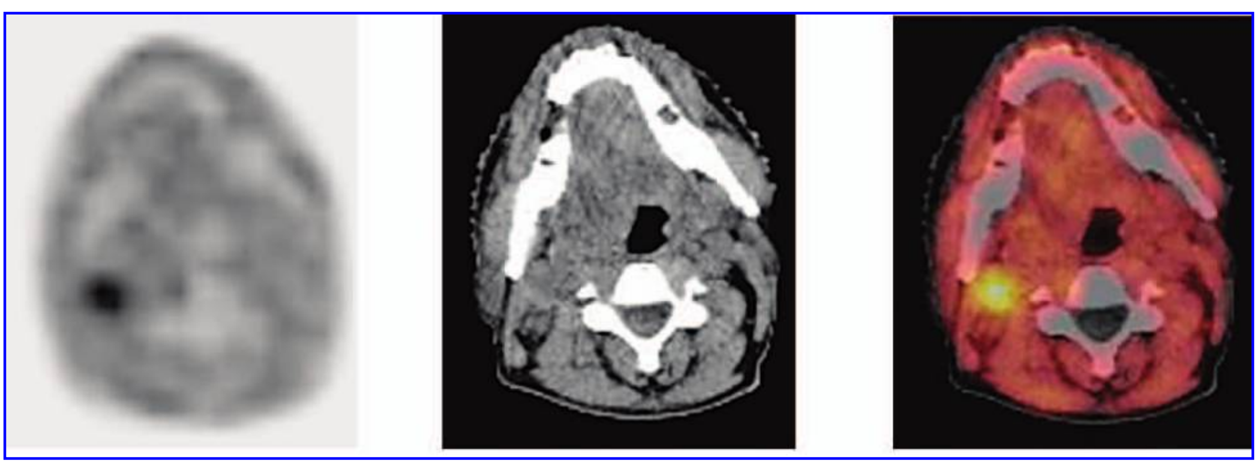

A B C

FIG. 3. PET and PET/CT imaging using radio-labeled hypoxia markers. The images were acquired from a patient with squamous cell carcinoma of the pharynx. (**A**) shows the PET image with FAZA uptake. (**B**) shows the corresponding CT image. (**C**) shows the PET/CT image. Reproduced with permission from Krouse *et al*. (44). (For interpretation of the references to color in this figure legend, the reader is referred to the web version of this article at www.liebertonline.com/ars)

review articles on the advantages and issues of EF5 PET imaging for hypoxia are available in the literature (40).

In certain cases, a long half-life (such as 12 h for EF5) may result in binding to aerobic cells and slower excretion of the unmetabolized marker from normal tissues. This will result in interference in obtaining a hypoxic-specific image (40). Consequently, tracers like ^{18}F FAZA have been developed to overcome this problem (44). Figure 3 shows a representative PET and PET/CT imaging using a FAZA obtained from a patient with squamous cell carcinoma of the pharynx. In general, specificity and reduction due to nonoxygenation-related processes are critical issues for interpretation of PET data.

PET imaging has been extensively used in tumor models for hypoxia mapping, as well as in clinical cases. Hypoxic tumors have been imaged in mice (7, 51, 97), rats (20), and rabbits (58). Clinical studies include head and neck cancer (31, 66, 95) and lung cancer (25). A general review by Krause *et al.* covers PET imaging for hypoxia (44).

PET oximetry using FMISO has been compared with that of polarographic needle electrodes for human soft tissue sarcomas (8). It was concluded that PET does not measure hypoxia to the same extent as that reported by electrode measurements. Several possibilities with regards to the differences were discussed, with one being the nonidentification of cells that had a pO_2 of $>$2–3 mm Hg. The use of pimonidazole markers would have an advantage in this case because of their specificity to severe hypoxia. Piert *et al.* have reported oxygen measurements on normal pig livers correlated with polarographic needle electrode measurements (62).

^{19}F Magnetic resonance imaging

In 1988, Busse *et al.* (13) showed that the ^{19}F nuclear magnetic resonance (NMR) spin-lattice relaxation rate (R_1) of perfluorocarbon probes could be used for imaging tumor pO_2 *in vivo*. The technique is based on NMR, but unlike conventional MRI (proton imaging), a probe based on perfluorocarbons (PFCs) is used. The PFCs are infused intravenously in the form of emulsions (96). The ^{19}F spin lattice relaxation rate (R1) of PFCs varies linearly with the dissolved oxygen concentration. Thus, the ^{19}F-based oximetry reports absolute values of oxygen concentration. Another widely used PFC is perfluoro-15-crown-5-ether (15C5) (96). Using this technique, it is possible to image pO_2 as well as follow dynamic changes in tumors. It is possible to combine the ^{19}F images and ^{1}H anatomical images so that oxygen information, as well as its anatomical location, are provided for spatial registration. The modulation of tumor hypoxia and pO_2 measurements using this method has been found to be consistent with modified tumor response to irradiation (98).

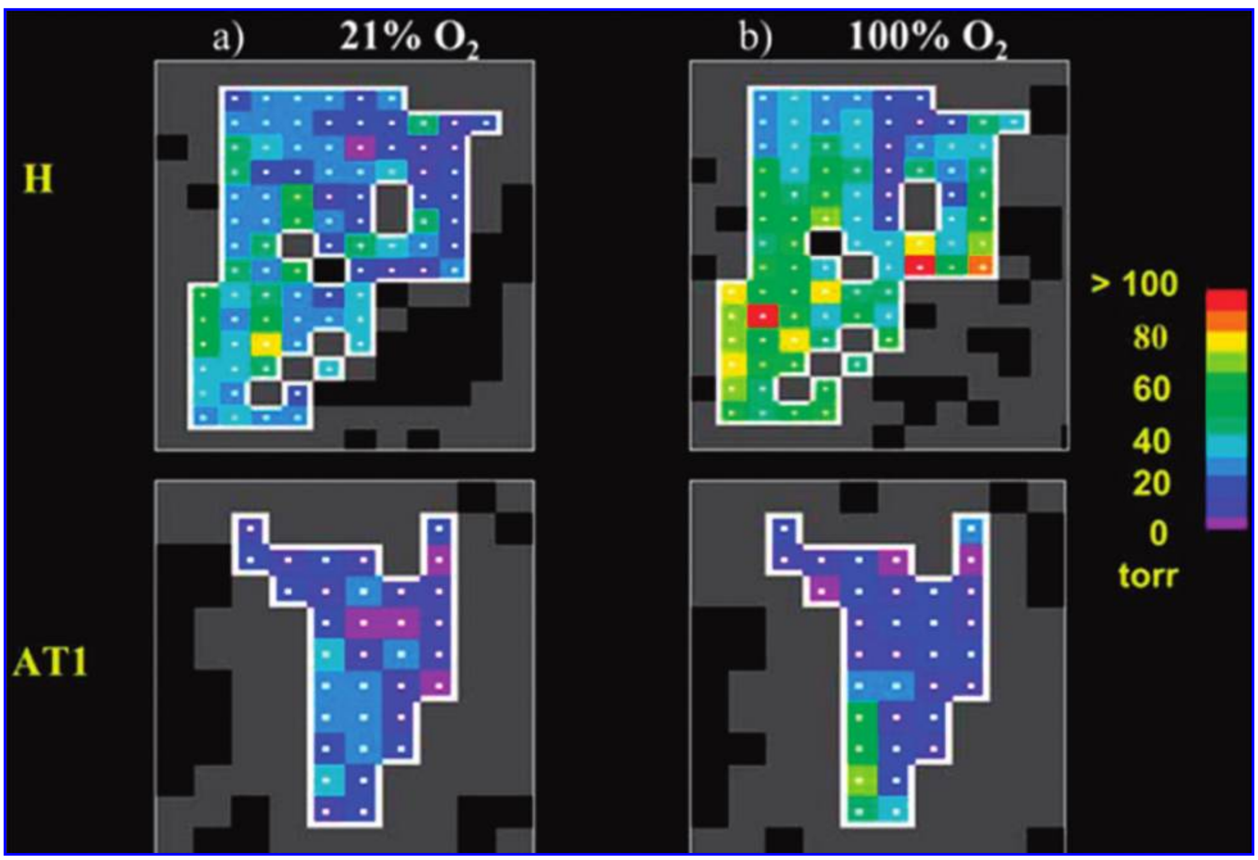

FIG. 4. Oxygen mapping of rat tumors using ^{19}F MRI. pO_2 maps of rat tumors obtained using ^{19}F MRI using HFB (50 μL) as probe. The tumor shown in the **H** panel was better oxygenated compared to the tumor in **AT1.**The response to oxygen inhalation is also seen as the increase in the pO_2 in the well-oxygenated regions. Reproduced with permission from Yu *et al.* (96). (For interpretation of the references to color in this figure legend, the reader is referred to the web version of this article at www.liebertonline.com/ars)

PFCs have low toxicity and therefore can be injected intravenously (68). It is possible to encapsulate PFCs in oxygen-permeable shields that are biocompatible and can remain in tissue for a long time. This enables multiple readouts and repetitive imaging from the same site (68).

Mason *et al*. (54) used HFB (hexafluorobenzene) because it gives a single, narrow ^{19}F NMR signal. HFB is particularly advantageous for pO_2 measurements because of its high sensitivity to oxygen concentration and lack of temperature dependence compared to the rest of the PFCs (96). In addition, a long spin-spin relaxation time (T_2), availability, low cost, and easy storage contribute to HFB being the most widely used PFC in ^{19}F MRI imaging (96). HFB is retained in the tumor for hours (half life, 10 h), so repeated and dynamic measurements are possible. Use of echo planar imaging for the ^{19}F MRI of HFB can give as many as 150 pO_2 measurements in ~7 min.

Oxygen maps of rat tumors using HFB and ^{19}F MRI are shown in Fig. 4. A further advantage is that the oxygen sensitivity of PFCs is not affected by emulsification, dilution, pH, common proteins, and blood (96).

The PFCs can percolate into interstitial spaces within a tumor, but could also be forced out due to high interstitial pressure (68). However, this problem does not occur with encapsulated PFCs. The distribution of the probe is a disadvantage. The calibration curve used for tumor pO_2 maps from ^{19}F-T_1 relaxation maps are *in vitro* curves. However, it is believed that these curves hold for *in vivo* measurements as well (96). Temperature corrections need to be applied for PFCs other than HFB (56, 96).

The signal-to-noise ratio (SNR) at 1.5 T is one-third that of 4.7 T (68). While 4.7 T scanners are used primarily for research purposes, clinical evaluations are mostly performed at 1.5 T. Thus, larger doses might have to be used at lower magnetic fields and therefore, the toxicity of PFCs must be fully characterized before using for clinical applications.

HFB has been used in rodent models for different types of tumors including breast, prostate, and human lymphoma xenograft (96). Studies have also been conducted in rat brain, lung, and human eye (96). Yu *et al*. have reviewed ^{19}F MRI for physiology and pharmacology, of which tissue oxygenation is a part (96).

The ^{19}F MRI oximetry has been compared with the polarographic needle electrode (55). It was found that basal tumor pO_2 using ^{19}F oximetry was higher than those reported by the electrode. However, direct intratumoral administration of PFCs have produced histograms comparable to those produced by electrodes (57). ^{19}F MRI oximetry has also been compared with the fiberoptic measurement system OxyLite, which is a method for point measurements of pO_2 but not imaging. It was found that both methods were similar when the mice were breathing either oxygen or carbogen (99). A comparison with NIRS in a tumor model has also been reported and it was found that changes in vascular oxygenation (obtained using NIRS) were more rapid compared to tumor pO_2 measurements using ^{19}F MRI (93).

BOLD imaging

Thulborn *et al*. first demonstrated the variation of the relaxation time, T_2, of protons with the level of blood oxygenation (76). Ogawa *et al*. first described blood oxygen level-dependent (BOLD) MRI for tissues for imaging the blood oxygen level in rat brains (59, 60). Further studies were performed in cat brains (78). BOLD images reflect the changes in the amount of oxygen bound to hemoglobin in blood. Deoxyhemoglobin is paramagnetic while oxyhemoglobin is not. The deoxyhemoglobin content in blood can cause differences in susceptibility (*i.e*., changes in the local magnetic field) around the blood vessels. This affects the relaxation properties of the surrounding protons. Thus, a decrease in MRI image signal intensity reflects a decrease in the blood oxygenation. In terms of relaxation parameters, the spin–lattice relaxation rate R1 is not affected by changes in oxygenation, while the spin–spin relaxation parameters R_2 and R_2* (where R_2* incorporates local field inhomogeneities) are both affected (53).

Assessment of oxygen is performed by BOLD MRI and hence it is noninvasive. It can be performed using the available clinical scanners and has the advantage of the availability of fast imaging sequences. It can also provide temporal information when various oxygenation treatments are used (6). The repeatability and voxel-by-voxel information about changes in blood oxygenation, co-registered with anatomical information are also advantages over other imaging techniques.

A major disadvantage of the BOLD oximetry is that it does not provide quantitative blood oxygenation information (6). It measures the changes in blood oxygenation, but not the absolute oxygen concentration in tissue. The data are also affected by other factors, such as the macroscopic field inhomogeneity and the R2 relaxation process. The deoxyhemoglobin content can be affected by the local blood flow and volume, and this must be taken into account when interpreting the data (6, 53). In addition, hematocrit concentration, pH, and temperature can

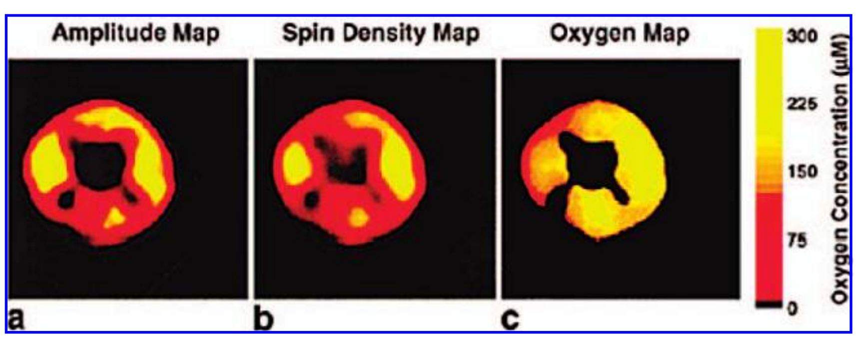

FIG. 5. Image of oxygen distribution in the cross-section of a rat tail. The image was reconstructed from 3D spectral-spatial data obtained *in vivo* from a rat intravenously infused with 3-carbamoylproxyl (3-CP), a soluble oximetry probe. Certain anatomical features (major blood vessels) and oxygen gradients are prominent in the image. Reproduced with permission from Kuppusamy et al. (47). (For interpretation of the references to color in this figure legend, the reader is referred to the web version of this article at www.liebertonline.com/ars)

change the fraction of deoxyhemoglobin as a function of pO_2 and R_2* (53). The calibration for conversion of R_2* to tissue oxygenation is also not straightforward (6).

Most of the applications of BOLD studies have been for functional MRI (fMRI). BOLD MRI has been used for investigating the effects of carbogen-breathing in mice and tumor models (73). It has also been used for oxygenation measurements in the kidney in patients (77). Baudelet *et al*. (6) have compared BOLD contrast with pO_2 in tumors. The pO_2 was measured using OxyLite, the fiberoptic fluorescence method (6). It was found that while the BOLD signal temporally correlated with changes in pO_2, there was no correlation of the amplitude of the BOLD signal with absolute pO_2 in the tumors (6). A good correlation was found between the average increase in the T_2* signal and pO_2 measured using microelectrodes in a tumor model (4).

Electron paramagnetic resonance imaging

Electron paramagnetic resonance (EPR) spectroscopy, discovered in 1944 by Zavoisky, has the unique capability to detect materials containing unpaired electrons. In addition, it can also provide information about the local environment including oxygenation, and this aspect makes EPR spectroscopy and imaging (EPRI) extremely valuable. Some of the major applications of EPR *in vivo* are for imaging and measurement of oxygenation in hypoxic/ischemic tissue.

The measurement of oxygen concentration by EPR (EPR oximetry) involves the use of an external probe consisting of either implantable paramagnetic particulates, or soluble probes that physically interact with, but do not consume oxygen (74). The changes in the EPR linewidth caused by the interaction of two paramagnetic species, molecular oxygen and the probe, determine pO_2. The spin–spin relaxation rate, R2, of the probe increases with oxygen concentration. The increase in relaxation rate (R_2) implies that the spin–spin relaxation time of the probe (T_2) will decrease resulting in line-broadening (35).

EPRI data is collected using continuous-wave (CW) or pulse (time domain) spectrometers. Time domain EPRI requires probes that have a narrow linewidth and has advantages in terms of the speed of data acquisition (94). However, most EPRI studies are done using CW techniques which can detect species with narrow and broad linewidths. Unlike MRI, which uses electromagnetic radiation in the radiofrequency range and high magnetic fields, EPRI requires radiation in the microwave region (L-Band for *in vivo* applications, 1.2 GHz) and low magnetic field (~700 times less at the same frequency). Several groups have developed EPRI successfully at very low frequencies, in the range of 250–1,200 MHz (18, 86).

The mapping of oxygen concentration using EPR imaging involves the use of spectral-spatial (spectroscopic) imaging techniques where the image contains not only spatial information (the spatial distribution of spin density) but also spectral information (spatial distribution of oxygen concentration). The method requires stepped field gradients and the resulting image has information in one, two, or three spatial dimensions and one spectral dimension (47). Thus, a 4D spectral-spatial image has information about the signal amplitude along three spatial dimensions and linewidth information along the spectral dimension.

Imaging of oxygenation using EPRI has been performed in a rat tail (Fig. 5), with a soluble nitroxide probe, where the cross-sectional anatomy and oxygen distribution is evident (81). The oxygen map showed the differences in the oxygen perfusion, and the major blood vessels and muscle bundles separated by bone were visible. Oxygen gradients from the center of the four regions (major vessels) into the distal regions can be seen on the oxygen maps. Figure 6 shows images of a tumor, where the mouse was either breathing air or carbogen (24). These images, obtained at 250 MHz, show the heterogeneity in the distribution of oxygen.

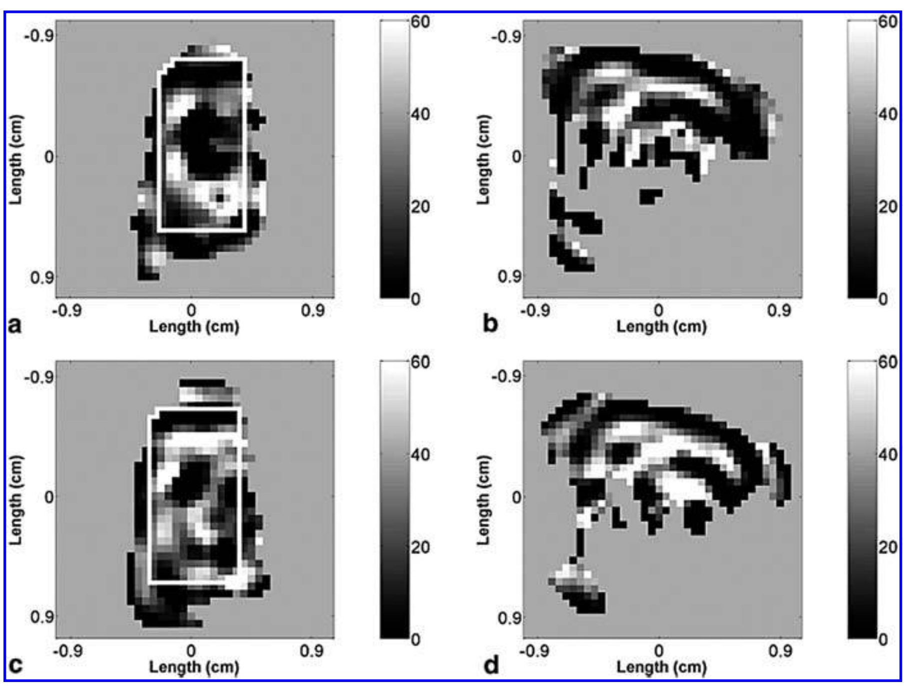

FIG. 6. EPRI oxygen image of an FSa tumor in the leg of a mouse. The distribution of oxygen is shown in a coronal (**a**) and sagittal (**b**) slice of the tumor in the leg of an air-breathing mouse. The images (**c**) and (**d**) represent the corresponding slices in the same tumor after carbogen-breathing for 10 min. The *intensity bar to the right* of each image quantifies oxygenation in torr. The oxygen distributions (**c**) and (**d**) are similar to that in (**a**) and (**b**). Overall, it is clear that the pO_2 values in (**c**) and (**d**) are higher. Reproduced with permission from Elas *et al*. (24).

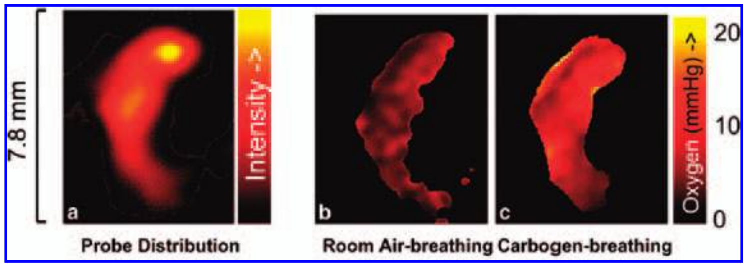

FIG. 7. Oxygen images of a RIF-1 tumor in mouse under normal air breathing and carbogen breathing conditions. The EPR images were obtained from a RIF-1 (radiation-induced fibrosarcoma) tumor embedded with particulates of lithium phthalocyanine (LiPc) oximetry probe. The images were obtained on day 11 after the animal was inoculated with LiPc and RIF-1 cells. (**a**) Spatial image showing the distribution of the particulates in the tumor. (**b**) Oxygen image, obtained from spectroscopic imaging, of the tumor in a room-air-breathing animal. (**c**) Oxygen image of the tumor under carbogen-breathing conditions. The overall increase in intensity in the carbogen-breathing animal Ilangovan *et al*. (34). (For interpretation of the references to color in this figure legend, the reader is referred to the web version of this article at www.liebertonline.com/ars)

Figure 7 shows an example of oxygen mapping in a murine tumor (34). In this case, nanoparticulate probes of LiPc were coimplanted with RIF-1 tumor cells into a mouse leg. This implanted probe enabled repeated measurements of the oxygenation status in the tumor for >2 weeks during the growth phase. The images shown in Fig. 7 reveal increases in tumor oxygenation during carbogen (95% O_2 and 5% CO_2) breathing by the mouse. The particulate probes have higher sensitivity than the available soluble probes (27).

A new imaging modality called PEDRI (proton electron double resonance imaging) or OMRI (Overhauser-enhanced magnetic resonance imaging) has been reported for oxygen imaging (48). This technique is also capable of imaging oxygenation in tissue. This method also requires the injection of an external probe that has unpaired electrons. Briefly, a strong EPR pulse saturates EPR resonance and results in the dipolar coupling of electrons and protons that causes an increase in the polarization of the protons, thereby enhancing the MRI signal intensity (48). This enhancement is affected by the presence of paramagnetic oxygen molecules. Figure 8 shows OMRI images of a mouse with a tumor showing the heterogeneity in the tumor region (45). The probe used for this experiment was Ox063, a soluble probe. The increase in pO_2 in the tumor when the mouse was breathing carbogen is evident. The study shows that OMRI can be used for dynamic studies of oxygen measurement (45).

EPR oximetry is a minimally invasive method that reports direct and absolute pO_2 or O_2 concentration in intact biological tissue (21). It has high sensitivity to pO_2 and has the capability for localized mapping if needed. There is very little interference from other sources (high specificity), no toxicity, and is not affected by the environment. The probes are nontoxic, with a reasonable half-life and adequate distribution in tissue. Qualitative, as well as quantitative pO_2 readings can be obtained using this technique. The most important advantage is being

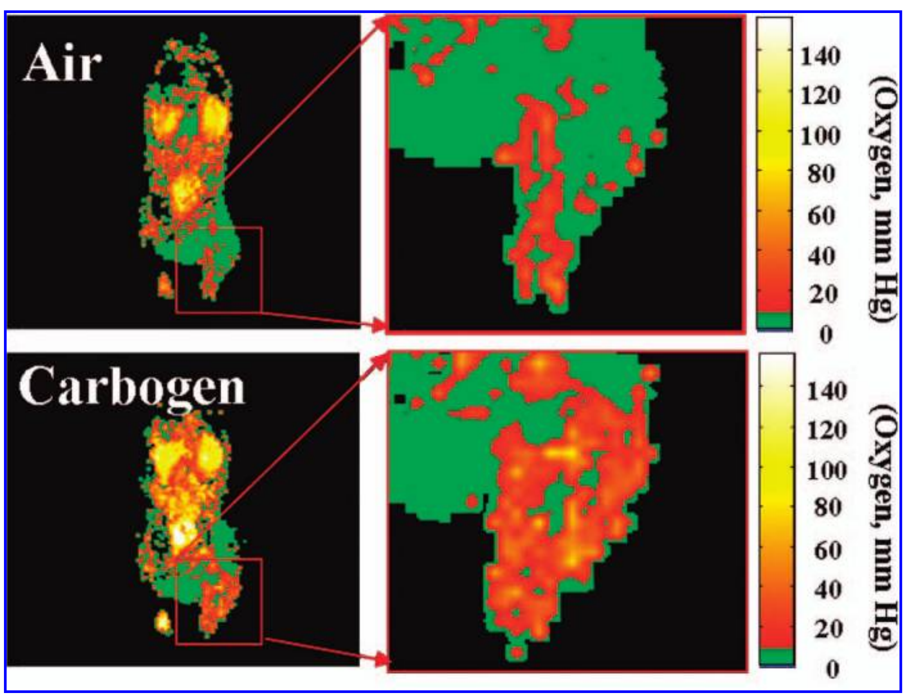

FIG. 8. OMRI oxygen images. The images were obtained from the tumor (SCC, squamous cell carcinoma) of a mouse under air- and carbogen-breathing conditions. The expanded tumor region, given at *right*, clearly shows heterogeneity in pO_2 distribution. Although the oxygen status in the tumor reveals severely hypoxic regions, increase in the pO_2 status in response to carbogen-breathing was observed. Reproduced with permission from Krishna *et al*. (45). (For interpretation of the references to color in this figure legend, the reader is referred to the web version of this article at www.liebertonline.com/ars)

able to take repeated measurements so that monitoring of oxygenation status is possible, though this is limited by the duration of retention of the probe in the tissue (27).

Data acquisition time is a major issue in EPRI. A reasonable 3D spectral-spatial image takes ~30 min (47). Soluble probes are used for imaging, which have low sensitivity compared to particulate probes. However, improvements in image reconstruction algorithms have considerably reduced data acquisition time for spatial imaging and these will be extended to spectral-spatial imaging in the near future (2, 3, 18). The penetration depth is several millimeters at 1.2 GHz, but higher at lower frequencies.

Spectral-spatial imaging has been used to investigate tumor oxygenation, and numerous examples described earlier in this article show the usefulness, repeatability, and suitability for dynamic studies. In addition to tumor imaging, EPRI has also been used for skin imaging applications and imaging of ischemic hearts (29, 46, 47). Oxygen imaging using EPRI has been compared with BOLD MRI by Elas *et al*. (24). A good spatial correlation between the two methods was found using mouse tumor models under normal air breathing and carbogen breathing conditions. EPR and OxyLite have also been compared by Elas *et al*. (23) in FSa fibrosarcomas implanted in the right hind limbs of nine C3H mice. Their study showed a good correlation between pO_2 measurements using OxyLite and EPR spectral-spatial imaging of the tumor.

EPRI is particularly suited for wound imaging because of its high sensitivity, resolution, and suitability for topical imaging. The added advantage of being able to take repeated measurements enable dynamic investigations and monitoring of therapy that will be useful when studying wound healing, cardiovascular diseases, and peripheral vascular diseases. The technique is currently undergoing major advances with respect to probe development, as well as data acquisition time and instrumentation that will make EPRI useful for a wide variety of applications.

SUMMARY AND CONCLUSIONS

Although the methods discussed above differ in their ability to provide spatially resolved information (mapping) of tissue oxygenation, they are very complementary in nature. As we know, tissue oxygenation is very heterogeneous which includes highly oxygenated arterial vascular regions to poorly oxygenated tissues and cells far away from them. In addition, the requirements for the diagnosis, therapies, and prediction of treatment outcome are so different that no one method will satisfy all the needs. This is particularly true with all of the above methods of imaging tissue oxygenation which differ significantly from each other in terms of parameter measured, invasiveness, accuracy, ease-of-use, and applicability for use in human. Nevertheless, there are concerted efforts in the development of novel imaging modalities and probes for imaging of tissue oxygenation.

ACKNOWLEDGMENTS

This work was supported by National Institutes of Health Grant EB005004. We would like to thank Nancy Trigg and Brian Rivera for critical reading of the manuscript.

REFERENCES

1. Abele D. Toxic oxygen: the radical life-giver. *Nature* 420: 27, 2002.
2. Ahmad R, Clymer B, Deng Y, He G, Vikram D, Kuppusamy P, and Zweier JL. Optimization of data acquisition for EPR imaging. *J Magn Reson* 179: 263–272, 2006.
3. Ahmad R, Deng Y, Vikram DS, Clymer B, Srinivasan P, Zweier JL, and Kuppusamy P. Quasi Monte Carlo-based isotropic distribution of gradient directions for improved reconstruction quality of 3D EPR imaging. *J Magn Reson* 184: 246–257, 2007..
4. Al–Hallaq HA, River JN, Zamora M, Oikawa H, and Karczmar GS. Correlation of magnetic resonance and oxygen microelectrode measurements of carbogen-induced changes in tumor oxygenation. *Int J Radiat Oncol Biol Phys* 41: 151–159, 1998.
5. Alavi A. PET imaging II. *Radiol Clin North Am* 43: xiii–xv, 2005.
6. Baudelet C and Gallez B. How does blood oxygen level-dependent (BOLD) contrast correlate with oxygen partial pressure (pO_2) inside tumors? *Magn Reson Med* 48: 980–986, 2002.
7. Bentzen L, Keiding S, Horsman MR, Gronroos T, Hansen SB, and Overgaard J. Assessment of hypoxia in experimental mice tumours by [18F]fluoromisonidazole PET and pO2 electrode measurements. Influence of tumour volume and carbogen breathing. Acta Oncol 41: 304–312, 2002.
8. Bentzen L, Keiding S, Nordsmark M, Falborg L, Hansen SB, Keller J, Nielsen OS, and Overgaard J. Tumour oxygenation assessed by 18F-fluoromisonidazole PET and polarographic needle electrodes in human soft tissue tumours. *Radiother Oncol* 67: 339–344, 2003.
9. Boushel R, Langberg H, Olesen J, Gonzales–Alonzo J, Bulow J, and Kjaer M. Monitoring tissue oxygen availability with near infrared spectroscopy (NIRS) in health and disease. *Scand J Med Sci Sports* 11: 213–222, 2001.
10. Boushel R and Piantadosi CA. Near-infrared spectroscopy for monitoring muscle oxygenation. *Acta Physiol Scand* 168: 615–622, 2000.
11. Brizel DM, Rosner GL, Prosnitz LR, and Dewhirst MW. Patterns and variability of tumor oxygenation in human soft tissue sarcomas, cervical carcinomas, and lymph node metastases. *Int J Radiat Oncol Biol Phys* 32: 1121–1125, 1995.
12. Brizel DM, Scully SP, Harrelson JM, Layfield LJ, Bean JM, Prosnitz LR, and Dewhirst MW. Tumor oxygenation predicts for the likelihood of distant metastases in human soft tissue sarcoma. *Cancer Res* 56: 941–943, 1996.
13. Busse LJ, Pratt RG, and Thomas SR. Deconvolution of chemical shift spectra in two- or three-dimensional [19F] MR imaging. *J Comput Assist Tomogr* 12: 824–835, 1988.
14. Cater DB and Silver IA. Quantitative measurements of oxygen tension in normal tissues and in the tumours of patients before and after radiotherapy. *Acta Radiol* 53: 233–256, 1960.
15. Chance B, Luo Q, Nioka S, Alsop DC, and Detre JA. Optical investigations of physiology: a study of intrinsic and extrinsic biomedical contrast. *Philos Trans R Soc Lond B Biol* Sci 352: 707–716, 1997.
16. Chapman JD, Engelhardt EL, Stobbe CC, Schneider RF, and Hanks GE. Measuring hypoxia and predicting tumor radioresistance with nuclear medicine assays. *Radiother Oncol* 46: 229–237, 1998.
17. Clarkson AN, Sutherland BA, and Appleton I. The biology and pathology of hypoxia-ischemia: an update. *Arch Immunol Ther Exp* (*Warsz*) 53: 213–225, 2005.
18. Deng Y, He G, Petryakov S, Kuppusamy P, and Zweier JL. Fast EPR imaging at 300 MHz using spinning magnetic field gradients. *J Magn Reson* 168: 220–227, 2004.
19. Dewhirst MW, Klitzman B, Braun RD, Brizel DM, Haroon ZA, and Secomb TW. Review of methods used to study oxygen transport at the microcirculatory level. *Int J Cancer* 90: 237–255, 2000.
20. Dubois L, Landuyt W, Haustermans K, Dupont P, Bormans G, Vermaelen P, Flamen P, Verbeken E, and Mortelmans L. Evaluation of hypoxia in an experimental rat tumour model by [(18)F]fluoromisonidazole PET and immunohistochemistry. *Br J Cancer* 91: 1947–1954, 2004.
21. Dunn JF and Swartz HM. *In vivo* electron paramagnetic resonance oximetry with particulate materials. *Methods* 30: 159–166, 2003.
22. Dunn JF, Zaim–Wadghiri Y, Pogue BW, and Kida I. BOLD MRI vs. NIR spectrophotometry. Will the best technique come forward? *Adv Exp Med Biol* 454: 103–113, 1998.

23. Elas M, Ahn KH, Parasca A, Barth ED, Lee D, Haney C, and Halpern HJ. Electron paramagnetic resonance oxygen images correlate spatially and quantitatively with Oxylite oxygen measurements. *Clin Cancer Res* 12: 4209–4217, 2006.
24. Elas M, Williams BB, Parasca A, Mailer C, Pelizzari CA, Lewis MA, River JN, Karczmar GS, Barth ED, and Halpern HJ. Quantitative tumor oxymetric images from 4D electron paramagnetic resonance imaging (EPRI): methodology and comparison with blood oxygen level-dependent (BOLD) MRI. *Magn Reson Med* 49: 682–691, 2003.
25. Eschmann SM, Paulsen F, Reimold M, Dittmann H, Welz S, Reischl G, Machulla HJ, and Bares R. Prognostic impact of hypoxia imaging with 18F-misonidazole PET in non-small cell lung cancer and head and neck cancer before radiotherapy. *J Nucl Med* 46: 253–260, 2005.
26. Fukumura D, Xu L, Chen Y, Gohongi T, Seed B, and Jain RK. Hypoxia and acidosis independently up-regulate vascular endothelial growth factor transcription in brain tumors *in vivo*. *Cancer Res* 61: 6020–6024, 2001.
27. Gallez B, Baudelet C, and Jordan BF. Assessment of tumor oxygenation by electron paramagnetic resonance: principles and applications. *NMR Biomed* 17: 240–262, 2004.
28. Graham MM, Peterson LM, Link JM, Evans ML, Rasey JS, Koh WJ, Caldwell JH, and Krohn KA. Fluorine-18-fluoromisonidazole radiation dosimetry in imaging studies. *J Nucl Med* 38: 1631–1636, 1997.
29. He G, Samouilov A, Kuppusamy P, and Zweier JL. *In vivo* EPR imaging of the distribution and metabolism of nitroxide radicals in human skin. *J Magn Reson* 148: 155–164, 2001.
30. Hebden JC, Gibson A, Yusof RM, Everdell N, Hillman EM, Delpy DT, Arridge SR, Austin T, Meek JH, and Wyatt JS. Three-dimensional optical tomography of the premature infant brain. *Phys Med Biol* 47: 4155–4166, 2002.
31. Hicks RJ, Rischin D, Fisher R, Binns D, Scott AM, and Peters LJ. Utility of FMISO PET in advanced head and neck cancer treated with chemoradiation incorporating a hypoxia-targeting chemotherapy agent. *Eur J Nucl Med Mol Imaging* 32: 1384–1391, 2005.
32. Hockel M, Knoop C, Schlenger K, Vorndran B, Baussmann E, Mitze M, Knapstein PG, and Vaupel P. Intratumoral pO_2 predicts survival in advanced cancer of the uterine cervix. *Radiother Oncol* 26: 45–50, 1993.
33. Hockel M, Schlenger K, Aral B, Mitze M, Schaffer U, and Vaupel P. Association between tumor hypoxia and malignant progression in advanced cancer of the uterine cervix. *Cancer Res* 56: 4509–4515, 1996.
34. Ilangovan G, Bratasz A, Li H, Schmalbrock P, Zweier JL, and Kuppusamy P. In vivo measurement and imaging of tumor oxygenation using coembedded paramagnetic particulates. *Magn Reson Med* 52: 650–657, 2004.
35. Ilangovan G, Zweier JL, and Kuppusamy P. Mechanism of oxygen-induced EPR line broadening in lithium phthalocyanine microcrystals. *J Magn Reson* 170: 42–48, 2004.
36. Intes X and Chance B. Non-PET functional imaging techniques: optical. *Radiol Clin North Am* 43: 221–234, xii, 2005.
37. Jobsis FF. Noninvasive, infrared monitoring of cerebral and myocardial oxygen sufficiency and circulatory parameters. *Science* 198: 1264–1267, 1977.
38. Kida I, Yamamoto T, and Tamura M. Interpretation of BOLD MRI signals in rat brain using simultaneously measured near-infrared spectrophotometric information. *NMR Biomed* 9: 333–338, 1996.
39. Kirkpatrick PJ, Lam J, Al–Rawi P, Smielewski P, and Czosnyka M. Defining thresholds for critical ischemia by using near-infrared spectroscopy in the adult brain. *J Neurosurg* 89: 389–394, 1998.
40. Koch CJ and Evans SM. Non-invasive PET and SPECT imaging of tissue hypoxia using isotopically labeled 2-nitroimidazoles. *Adv Exp Med Biol* 510: 285–292, 2003.
41. Koh WJ, Bergman KS, Rasey JS, Peterson LM, Evans ML, Graham MM, Grierson JR, Lindsley KL, Lewellen TK, Krohn KA, et al. Evaluation of oxygenation status during fractionated radiotherapy in human nonsmall cell lung cancers using [F-18]fluoromisonidazole positron emission tomography. *Int J Radiat Oncol Biol Phys* 33: 391–398, 1995.
42. Koh WJ, Rasey JS, Evans ML, Grierson JR, Lewellen TK, Graham MM, Krohn KA, and Griffin TW. Imaging of hypoxia in human tumors with [F-18]fluoromisonidazole. *Int J Radiat Oncol Biol Phys* 22: 199–212, 1992.
43. Kolstad P. Intercapillary distance, oxygen tension and local recurrence in cervix cancer. *Scand J Clin Lab Invest Suppl* 106: 145–157, 1968.
44. Krause BJ, Beck R, Souvatzoglou M, and Piert M. PET and PET/CT studies of tumor tissue oxygenation. *Q J Nucl Med Mol Imaging* 50: 28–43, 2006.
45. Krishna MC, English S, Yamada K, Yoo J, Murugesan R, Devasahayam N, Cook JA, Golman K, Ardenkjaer-Larsen JH, Subramanian S, and Mitchell JB. Overhauser enhanced magnetic resonance imaging for tumor oximetry: coregistration of tumor anatomy and tissue oxygen concentration. *Proc Natl Acad Sci USA* 99: 2216–2221, 2002.
46. Kuppusamy P, Chzhan M, Wang P, and Zweier JL. Three-dimensional gated EPR imaging of the beating heart: time-resolved measurements of free radical distribution during the cardiac contractile cycle. *Magn Reson Med* 35: 323–328, 1996.
47. Kuppusamy P, Shankar RA, and Zweier JL. *In vivo* measurement of arterial and venous oxygenation in the rat using 3D spectral-spatial electron paramagnetic resonance imaging. *Phys Med Biol* 43: 1837–1844, 1998.
48. Liebgott T, Li H, Deng Y, and Zweier JL. Proton electron double resonance imaging (PEDRI) of the isolated beating rat heart. *Magn Reson Med* 50: 391–399, 2003.
49. Lo LW, Jenkins WT, Vinogradov SA, Evans SM, and Wilson DF. Oxygen distribution in the vasculature of mouse tissue in vivo measured using a near infra red phosphor. *Adv Exp Med Biol* 411: 577–583, 1997.
50. Loi S, Ngan SY, Hicks RJ, Mukesh B, Mitchell P, Michael M, Zalcberg J, Leong T, Lim-Joon D, Mackay J, and Rischin D. Oxaliplatin combined with infusional 5-fluorouracil and concomitant radiotherapy in inoperable and metastatic rectal cancer: a phase I trial. *Br J Cancer* 92: 655–661, 2005.
51. Mannan RH, Somayaji VV, Lee J, Mercer JR, Chapman JD, and Wiebe LI. Radioiodinated 1-(5-iodo-5-deoxy-beta-D-arabinofuranosyl)-2-nitroimidazole (iodoazomycin arabinoside: IAZA): a novel marker of tissue hypoxia. *J Nucl Med* 32: 1764–1770, 1991.
52. Mariani E, Polidori MC, Cherubini A, and Mecocci P. Oxidative stress in brain aging, neurodegenerative and vascular diseases: an overview. *J Chromatogr B Analyt Technol Biomed Life Sci* 827: 65–75, 2005.
53. Mason RP. Non-invasive assessment of kidney oxygenation: a role for BOLD MRI. *Kidney Int* 70: 10–11, 2006.
54. Mason RP, Antich PP, Babcock EE, Constantinescu A, Peschke P, and Hahn EW. Non-invasive determination of tumor oxygen tension and local variation with growth. *Int J Radiat Oncol Biol Phys* 29: 95–103, 1994.
55. Mason RP, Constantinescu A, Hunjan S, Le D, Hahn EW, Antich PP, Blum C, and Peschke P. Regional tumor oxygenation and measurement of dynamic changes. *Radiat Res* 152: 239–249, 1999.
56. Mason RP, Rodbumrung W, and Antich PP. Hexafluorobenzene: a sensitive ^{19}F NMR indicator of tumor oxygenation. *NMR Biomed* 9: 125–134, 1996.
57. McIntyre DJO, McCoy,C.L and Griffiths,J.R. Tumor oxygenation measurements by 19F MRI of perflurocarbons. *Current Science* 76: 753–762, 1999.
58. Obata A, Yoshimoto M, Kasamatsu S, Naiki H, Takamatsu S, Kashikura K, Furukawa T, Lewis JS, Welch MJ, Saji H, Yonekura Y, and Fujibayashi Y. Intra-tumoral distribution of (64)Cu-ATSM: a comparison study with FDG. *Nucl Med Biol* 30: 529–534, 2003.
59. Ogawa S and Lee TM. Magnetic resonance imaging of blood vessels at high fields: in vivo and in vitro measurements and image simulation. *Magn Reson Med* 16: 9–18, 1990.
60. Ogawa S, Lee TM, Kay AR, and Tank DW. Brain magnetic resonance imaging with contrast dependent on blood oxygenation. *Proc Natl Acad Sci USA* 87: 9868–9872, 1990.
61. Okunieff P, Ding I, Vaupel P, and Hockel M. Evidence for and against hypoxia as the primary cause of tumor aggressiveness. *Adv Exp Med Biol* 510: 69–75, 2003.
62. Piert M, Machulla H, Becker G, Stahlschmidt A, Patt M, Aldinger P, Dissmann PD, Fischer H, Bares R, Becker HD, and Lauchart W. Introducing fluorine-18 fluoromisonidazole positron emission tomography for the localisation and quantification of pig liver hypoxia. *Eur J Nucl Med* 26: 95–109, 1999.

63. Piert M, Machulla HJ, Becker G, Aldinger P, Winter E, and Bares R. Dependency of the [18F]fluoromisonidazole uptake on oxygen delivery and tissue oxygenation in the porcine liver. *Nucl Med Biol* 27: 693–700, 2000.
64. Punwani S, Cooper CE, Clemence M, Penrice J, Amess P, Thornton J, and Ordidge RJ. Correlation between absolute deoxyhaemoglobin [dHb] measured by near infrared spectroscopy (NIRS) and absolute R2′ as determined by magnetic resonance imaging (MRI). *Adv Exp Med Biol* 413: 129–137, 1997.
65. Rajendran JG, Wilson DC, Conrad EU, Peterson LM, Bruckner JD, Rasey JS, Chin LK, Hofstrand PD, Grierson JR, Eary JF, and Krohn KA. [(18)F]FMISO and [(18)F]FDG PET imaging in soft tissue sarcomas: correlation of hypoxia, metabolism and VEGF expression. *Eur J Nucl Med Mol Imaging* 30: 695–704, 2003.
66. Rasey JS, Koh WJ, Evans ML, Peterson LM, Lewellen TK, Graham MM, and Krohn KA. Quantifying regional hypoxia in human tumors with positron emission tomography of [18F]fluoromisonidazole: a pretherapy study of 37 patients. *Int J Radiat Oncol Biol Phys* 36: 417–428, 1996.
67. Rasey JS, Nelson NJ, Chin L, Evans ML, and Grunbaum Z. Characteristics of the binding of labeled fluoromisonidazole in cells in vitro. *Radiat Res* 122: 301–308, 1990.
68. Robinson SP and Griffiths JR. Current issues in the utility of ^{19}F nuclear magnetic resonance methodologies for the assessment of tumour hypoxia. *Philos Trans R Soc Lond B Biol Sci* 359: 987–996, 2004.
69. Rumsey WL, Pawlowski M, Lejavardi N, and Wilson DF. Oxygen pressure distribution in the heart in vivo and evaluation of the ischemic “border zone”. *Am J Physiol* 266: H1676–1680, 1994.
70. Rumsey WL, Vanderkooi JM, and Wilson DF. Imaging of phosphorescence: a novel method for measuring oxygen distribution in perfused tissue. *Science* 241: 1649–1651, 1988.
71. Shonat RD and Norige AS. Developing strategies for three-dimensional imaging of oxygen tension in the rodent retina. *Adv Exp Med Biol* 566: 173–178, 2005.
72. Stankovic MR, Maulik D, Rosenfeld W, Stubblefield PG, Kofinas AD, Gratton E, Franceschini MA, Fantini S, and Hueber DM. Role of frequency domain optical spectroscopy in the detection of neonatal brain hemorrhage–a newborn piglet study. *J Matern Fetal Med* 9: 142–149, 2000.
73. Stubbs M. Application of magnetic resonance techniques for imaging tumour physiology. *Acta Oncol* 38: 845–853, 1999.
74. Swartz HM. Using EPR to measure a critical but often unmeasured component of oxidative damage: oxygen. *Antioxid Redox Signal* 6: 677–686, 2004.
75. Swartz HM and Dunn JF. Measurements of oxygen in tissues: overview and perspectives on methods. *Adv Exp Med Biol* 530: 1–12, 2003.
76. Thulborn KR, Waterton JC, Matthews PM, and Radda GK. Oxygenation dependence of the transverse relaxation time of water protons in whole blood at high field. *Biochim Biophys Acta* 714: 265–270, 1982.
77. Tumkur SM, Vu AT, Li LP, Pierchala L, and Prasad PV. Evaluation of intra-renal oxygenation during water diuresis: a time-resolved study using BOLD MRI. *Kidney Int* 70: 139–143, 2006.
78. Turner R, Le Bihan D, Moonen CT, Despres D, and Frank J. Echo-planar time course MRI of cat brain oxygenation changes. *Magn Reson Med* 22: 159–166, 1991.
79. Vaupel P, Mayer A, and Hockel M. Tumor hypoxia and malignant progression. *Methods Enzymol* 381: 335–354, 2004.
80. Vaupel P, Schlenger K, Knoop C, and Hockel M. Oxygenation of human tumors: evaluation of tissue oxygen distribution in breast cancers by computerized O2 tension measurements. *Cancer Res* 51: 3316–3322, 1991.
81. Velan SS, Spencer RG, Zweier JL, and Kuppusamy P. Electron paramagnetic resonance oxygen mapping (EPROM): direct visualization of oxygen concentration in tissue. *Magn Reson Med* 43: 804–809, 2000.
82. Vinogradov SA, Fernandez–Seara MA, Dupan BW, and Wilson DF. A method for measuring oxygen distributions in tissue using frequency domain phosphorometry. *Comp Biochem Physiol A Mol Integr Physiol* 132: 147–152, 2002.
83. Vinogradov SA, Fernandez–Seara,M.A. and Wilson,D.F. Frequency domain instrument for measuring phosphorescence lifetime distributions in heterogenous samples. *Rev Sci Instr* 72: 3396–3406, 2001.
84. Vinogradov SA, Grosul P, Rozhkov V, Dunphy I, Shuman L, Dugan BW, Evans S, and Wilson DF. Oxygen distributions in tissue measured by phosphorescence quenching. *Adv Exp Med Biol* 510: 181–185, 2003.
85. Vinogradov SA, Lo LW, Jenkins WT, Evans SM, Koch C, and Wilson DF. Noninvasive imaging of the distribution in oxygen in tissue in vivo using near-infrared phosphors. *Biophys J* 70: 1609–1617, 1996.
86. Williams BB, al Hallaq H, Chandramouli GV, Barth ED, Rivers JN, Lewis M, Galtsev VE, Karczmar GS, and Halpern HJ. Imaging spin probe distribution in the tumor of a living mouse with 250 MHz EPR: correlation with BOLD MRI. *Magn Reson Med* 47: 634–638, 2002.
87. Wilson DF and Cerniglia GJ. Localization of tumors and evaluation of their state of oxygenation by phosphorescence imaging. *Cancer Res* 52: 3988–3993, 1992.
88. Wilson DF and Cerniglia GJ. Oxygenation of tumors as evaluated by phosphorescence imaging. *Adv Exp Med Biol* 345: 539–547, 1994.
89. Wilson DF, Pastuszko A, DiGiacomo JE, Pawlowski M, Schneiderman R, and Delivoria–Papadopoulos M. Effect of hyperventilation on oxygenation of the brain cortex of newborn piglets. *J Appl Physiol* 70: 2691–2696, 1991.
90. Wilson DF, Vinogradov S, Lo LW, and Huang L. Oxygen dependent quenching of phosphorescence: a status report. *Adv Exp Med Biol* 388: 101–107, 1996.
91. Wilson DF, Vinogradov SA, Grosul P, Kuroki A, and Bennett J. Imaging oxygen pressure in the retina of the mouse eye. *Adv Exp Med Biol* 566: 159–165, 2005.
92. Wilson DF, Vinogradov SA, Grosul P, Vaccarezza MN, Kuroki A, and Bennett J. Oxygen distribution and vascular injury in the mouse eye measured by phosphorescence-lifetime imaging. *Appl Opt* 44: 5239–5248, 2005.
93. Xia M, Kodibagkar V, Liu H, and Mason RP. Tumour oxygen dynamics measured simultaneously by near-infrared spectroscopy and ^{19}F magnetic resonance imaging in rats. *Phys Med Biol* 51: 45–60, 2006.
94. Yamada K, Murugesan R, Devasahayam N, Cook JA, Mitchell JB, Subramanian S, and Krishna MC. Evaluation and comparison of pulsed and continuous wave radiofrequency electron paramagnetic resonance techniques for in vivo detection and imaging of free radicals. *J Magn Reson* 154: 287–297, 2002.
95. Yeh SH, Liu RS, Wu LC, Yang DJ, Yen SH, Chang CW, Yu TW, Chou KL, and Chen KY. Fluorine-18 fluoromisonidazole tumour to muscle retention ratio for the detection of hypoxia in nasopharyngeal carcinoma. *Eur J Nucl Med* 23: 1378–1383, 1996.
96. Yu JX, Kodibagkar VD, Cui W, and Mason RP. ^{19}F: a versatile reporter for non-invasive physiology and pharmacology using magnetic resonance. *Curr Med Chem* 12: 819–848, 2005.
97. Zanzonico P, O’Donoghue J, Chapman JD, Schneider R, Cai S, Larson S, Wen B, Chen Y, Finn R, Ruan S, Gerweck L, Humm J, and Ling C. Iodine-124-labeled iodo-azomycin-galactoside imaging of tumor hypoxia in mice with serial microPET scanning. *Eur J Nucl Med Mol Imaging* 31: 117–128, 2004.
98. Zhao D, Constantinescu A, Chang CH, Hahn EW, and Mason RP. Correlation of tumor oxygen dynamics with radiation response of the dunning prostate R3327-HI tumor. *Radiat Res* 159: 621–631, 2003.
99. Zhao D, Constantinescu A, Hahn EW, and Mason RP. Tumor oxygen dynamics with respect to growth and respiratory challenge: investigation of the Dunning prostate R3327-HI tumor. *Radiat Res* 156: 510–520, 2001.

Address reprint requests to:
Periannan Kuppusamy, PhD
The Ohio State University
420 West 12th Ave, Room 114
Columbus, OH 43210

E-mail: kuppusamy.1@osu.edu

Date of first submission to ARS Central, April 27, 2007; date of acceptance, May 2, 2007.

This article has been cited by:

1. Xue Meng, Feng-Ming (Spring) Kong, Jinming Yu. 2011. Implementation of hypoxia measurement into lung cancer therapy. *Lung Cancer* . [CrossRef]
2. Makiko Suehiro, Guangbin Yang, Geralda Torchon, Ellen Ackerstaff, John Humm, Jason Koutcher, Ouathek Ouerfelli. 2011. Radiosynthesis of the tumor hypoxia marker [18F]TFMISO via O-[18F]trifluoroethylation reveals a striking difference between trifluoroethyl tosylate and iodide in regiochemical reactivity toward oxygen nucleophiles. *Bioorganic & Medicinal Chemistry* **19**:7, 2287-2297. [CrossRef]
3. Reut Avni, Batya Cohen, Michal Neeman. 2011. Hypoxic stress and cancer: imaging the axis of evil in tumor metastasis. *NMR in Biomedicine* n/a-n/a. [CrossRef]
4. Jesús Pacheco-Torres, Pilar López-Larrubia, Paloma Ballesteros, Sebastián Cerdán. 2011. Imaging tumor hypoxia by magnetic resonance methods. *NMR in Biomedicine* **24**:1, 1-16. [CrossRef]
5. Boris Epel, Subramanian V. Sundramoorthy, Eugene D. Barth, Colin Mailer, Howard J. Halpern. 2011. Comparison of 250 MHz electron spin echo and continuous wave oxygen EPR imaging methods for in vivo applications. *Medical Physics* **38**:4, 2045. [CrossRef]
6. Quentin Godechal, Bernard Gallez. 2011. The Contribution of Electron Paramagnetic Resonance to Melanoma Research. *Journal of Skin Cancer* **2011**, 1-6. [CrossRef]
7. Bénédicte F. Jordan, Bernard Gallez. 2010. Surrogate MR markers of response to chemo- or radiotherapy in association with co-treatments: a retrospective analysis of multi-modal studies. *Contrast Media & Molecular Imaging* **5**:6, 323-332. [CrossRef]
8. R. Ahmad, G. Caia, L.C. Potter, S. Petryakov, P. Kuppusamy, J.L. Zweier. 2010. In vivo multisite oximetry using EPR–NMR coimaging. *Journal of Magnetic Resonance* **207**:1, 69-77. [CrossRef]
9. S. Schreml, R.M. Szeimies, L. Prantl, S. Karrer, M. Landthaler, P. Babilas. 2010. Oxygen in acute and chronic wound healing. *British Journal of Dermatology* **163**:2, 257-268. [CrossRef]
10. Cameron Rink, Sashwati Roy, Mahmood Khan, Pavan Ananth, Periannan Kuppusamy, Chandan K Sen, Savita Khanna. 2010. Oxygen-sensitive outcomes and gene expression in acute ischemic stroke. *Journal of Cerebral Blood Flow & Metabolism* **30**:7, 1275-1287. [CrossRef]
11. Guruguhan Meenakshisundaram, Edward Eteshola, Aharon Blank, Stephen C. Lee, Periannan Kuppusamy. 2010. A molecular paramagnetic spin-doped biopolymeric oxygen sensor. *Biosensors and Bioelectronics* **25**:10, 2283-2289. [CrossRef]
12. Aharon Blank, Revital Halevy, Michael Shklyar, Lazar Shtirberg, Periannan Kuppusamy. 2010. ESR micro-imaging of LiNc-BuO crystals in PDMS: Spatial and spectral grain distribution. *Journal of Magnetic Resonance* **203**:1, 150-155. [CrossRef]
13. Ana Margarida Abrantes, Maria Elisa Silva Serra, Ana Cristina Gonçalves, Joana Rio, Bárbara Oliveiros, Mafalda Laranjo, António Manuel Rocha-Gonsalves, Ana Bela Sarmento-Ribeiro, Maria Filomena Botelho. 2010. Hypoxia-induced redox alterations and their correlation with 99mTc-MIBI and 99mTc-HL-91 uptake in colon cancer cells. *Nuclear Medicine and Biology* **37**:2, 125-132. [CrossRef]
14. Boris Epel, Chad R. Haney, Danielle Hleihel, Craig Wardrip, Eugene D. Barth, Howard J. Halpern. 2010. Electron paramagnetic resonance oxygen imaging of a rabbit tumor using localized spin probe delivery. *Medical Physics* **37**:6, 2553. [CrossRef]
15. Mohammad A. Yaseen, Vivek J. Srinivasan, Sava Sakadži#, Weicheng Wu, Svetlana Ruvinskaya, Sergei A. Vinogradov, David A. Boas. 2009. Optical monitoring of oxygen tension in cortical microvessels with confocal microscopy. *Optics Express* **17**:25, 22341. [CrossRef]
16. Caroline Diepart, Bénédicte F. Jordan, Bernard Gallez. 2009. A New EPR Oximetry Protocol to Estimate the Tissue Oxygen Consumption In Vivo. *Radiation Research* **172**:2, 220-225. [CrossRef]
17. Guruguhan Meenakshisundaram, Edward Eteshola, Ramasamy P. Pandian, Anna Bratasz, Stephen C. Lee, Periannan Kuppusamy. 2009. Fabrication and physical evaluation of a polymer-encapsulated paramagnetic probe for biomedical oximetry. *Biomedical Microdevices* **11**:4, 773-782. [CrossRef]
18. Guruguhan Meenakshisundaram, Edward Eteshola, Ramasamy P. Pandian, Anna Bratasz, Karuppaiyah Selvendiran, Stephen C. Lee, Murali C. Krishna, Harold M. Swartz, Periannan Kuppusamy. 2009. Oxygen sensitivity and biocompatibility of an implantable paramagnetic probe for repeated measurements of tissue oxygenation. *Biomedical Microdevices* **11**:4, 817-826. [CrossRef]
19. Judith C Sluimer, Mat J Daemen. 2009. Novel concepts in atherogenesis: angiogenesis and hypoxia in atherosclerosis. *The Journal of Pathology* **218**:1, 7-29. [CrossRef]

20. Edward Eteshola, Ramasamy P. Pandian, Stephen C. Lee, Periannan Kuppusamy. 2009. Polymer coating of paramagnetic particulates for in vivo oxygen-sensing applications. *Biomedical Microdevices* **11**:2, 379-387. [CrossRef]
21. N. Charlier, B. Driesschaert, N. Wauthoz, N. Beghein, V. Préat, K. Amighi, J. Marchand-Brynaert, B. Gallez. 2009. Nano-emulsions of fluorinated trityl radicals as sensors for EPR oximetry. *Journal of Magnetic Resonance* **197**:2, 176-180. [CrossRef]
22. S SCHNEIDER, H STRUDER. 2009. Monitoring effects of acute hypoxia on brain cortical activity by using electromagnetic tomography. *Behavioural Brain Research* **197**:2, 476-480. [CrossRef]
23. Deepti S. Vikram, Rizwan Ahmad, Brian K. Rivera, Periannan Kuppusamy. 2008. Mapping of Oxygen Concentration in Biological Samples Using EPR Imaging. *Israel Journal of Chemistry* **48**:1, 39-43. [CrossRef]
24. Deepti S. Vikram, Rizwan Ahmad, Ramasamy P. Pandian, Sergey Petryakov, Periannan Kuppusamy. 2008. Evaluation of oxygen-response times of phthalocyanine-based crystalline paramagnetic spin probes for EPR oximetry. *Journal of Magnetic Resonance* **193**:1, 127-132. [CrossRef]